Monthly Notices
of the
ROYAL ASTRONOMICAL SOCIETY

MNRAS **458,** 3684–3690 (2016)
Advance Access publication 2016 February 12

doi:10.1093/mnras/stw317

Study of a bright-rimmed cloud at the border of the infrared dust bubble CN20

M. E. Ortega,[1⋆] E. Giacani,[1,2] S. Paron[1,2,3] and M. Rubio[4]

[1] *Instituto de Astronomía y Física del Espacio (IAFE), CC 67, Suc. 28, 1428 Buenos Aires, Argentina*
[2] *FADU – Universidad de Buenos Aires, Ciudad Universitaria, Buenos Aires, Argentina*
[3] *CBC – Universidad de Buenos Aires, Ciudad Universitaria, Buenos Aires, Argentina*
[4] *Departamento de Astronomía, Universidad de Chile, Casilla 36-D, Santiago, Chile*

Accepted 2016 February 8. Received 2016 February 6; in original form 2015 November 5

ABSTRACT

We characterize an uncatalogued bright-rimmed cloud located at the border of the infrared dust bubble CN20 with the aim of investigating triggered star formation. In order to do this, we carried out radio continuum observations at 8.9 GHz using the Jansky Very Large Array (JVLA) interferometer with a synthesized beam size of 13 arcsec × 5 arcsec, and molecular observations using the Atacama Submillimeter Telescope Experiment (ASTE) at the ^{13}CO J = 3–2 and CS J = 7–6 transitions. An analysis of the molecular observations and of *Herschel* public data revealed the presence of a warm and dense clump with $T_{\rm dust} \sim 25$ K and $n(H_2) \sim 3 \times 10^5$ cm^{-3}. The high angular resolution and sensitivity of the new radio continuum data revealed an arc-like radio filament in excellent correspondence with the illuminated border of the bright-rimmed cloud. This ionized boundary layer has an electron density of 176 cm^{-3}. The spatial distribution of the young stellar object candidates probably related to the bright-rimmed cloud does not show clear evidence of a triggered origin. Finally, based on the evaluation of the pressure balance between the ionized and molecular gas, we conclude that the ionization front has stalled at the surface of the clump.

Key words: stars: formation – ISM: clouds – H II regions.

1 INTRODUCTION

Bright-rimmed clouds (BRCs) are isolated molecular clouds located at the edges of evolved H II regions with their illuminated borders facing towards the ionizing star(s). They are believed to be potential sites of triggered star formation (e.g. Sandford, Whitaker & Klein 1982; Bertoldi 1989; Lefloch & Lazareff 1994) through a mechanism known as radiation-driven implosion (RDI), which was first proposed by Reipurth (1983). BRCs are used as markers of the location of the ionization front of an H II region, which are not easy to define but are believed to contribute mainly as positive-feedback in the formation of new stars.

Sugitani, Fukui & Ogura (1991) and Sugitani & Ogura (1994) compiled optical catalogues (the so-called SFO Catalogues) of 44 BRCs in the northern sky and of 45 BRCs in the southern sky, each associated with an *IRAS* point source of low dust temperature. Detailed characterizations of the physical properties of some BRCs included in the SFO Catalogue were made based on submillimetre and radio continuum observations (e.g. Morgan et al. 2004; Thompson, Urquhart & White 2004; Urquhart et al. 2006; Morgan, Urquhart & Thompson 2009). Some authors have concluded that the RDI mechanism is in progress in many (but not all) of the SFO BRCs and that massive stars are being formed in these regions (Urquhart, Morgan & Thompson 2009). Studies such as those of Sugitani, Tamura & Ogura (1995) and Smith et al. (2010), which are based on infrared (IR) observations, indicate that BRCs are often associated with a small cluster of young stars showing not only an asymmetric spatial distribution with respect to the cloud but also a possible age gradient. Furthermore , several studies based on numerical simulations describe, with unprecedented detail, the physical conditions of BRCs, predicting where and when the new generation of stars should be formed (e.g. Gritschneder et al. 2010; Bisbas et al. 2011; Haworth et al. 2013; Kinnear et al. 2014). Haworth, Harries & Acreman (2012) have shown, based on synthetic observations derived from their numerical simulations, that the diagnostic tools used to analyse the evolution of the BRCs are reliable. However, distinguishing between triggered and spontaneously formed stars is not an easy task. Based on a statistical study of the spatial distributions of the IR dust bubbles catalogued by Churchwell et al. (2006) and the massive young stellar objects (MYSOs) catalogued in the Red MSX Source Survey (Urquhart et al. 2008), Thompson et al. (2012) suggested that the formation of about 14 to 30 per cent of the MYSOs in the Milky Way might have been triggered by the action of expanding bubbles/H II regions. As Dale, Haworth & Bressert (2015) point out, it is very important to interpret with caution the

⋆ E-mail: mortega@iafe.uba.ar

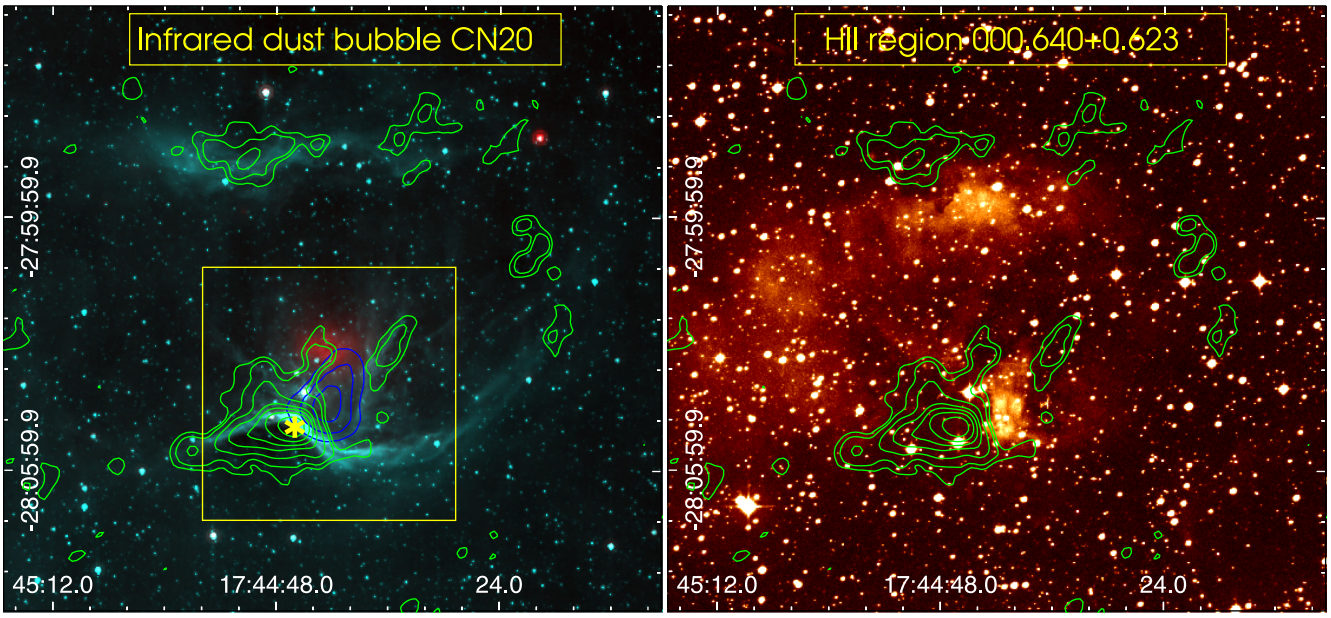

Figure 1. Left: Two-colour composite *Spitzer* image (8 μm in cyan and 24 μm in red) of the infrared dust bubble CN20 (infrared counterpart of the diffuse H II region G000.640+0.623). Cyan and red scales go from 60 to 200 MJy sr^{-1} and from 100 to 400 MJy sr^{-1}, respectively. The blue contours represent the radio continuum emission at 1.4 GHz extracted from the NVSS survey. Contours levels are at 0.004, 0.008 and 0.012 Jy beam^{-1}. The yellow box indicates the region mapped with the JVLA. The star represents the pointing of the ASTE observations. Right: H_α image of the H II region G000.640+0.623 as obtained from the SuperCOSMOS H_α Survey (SHS). The green contours in both images represent the ATLASGAL emission at 870 μm. Contour levels are at 0.02, 0.08, 0.15, 0.2, 0.3, 0.4 and 0.6 Jy beam^{-1}.

observations of star formation near feedback-driven structures such as BRCs in terms of triggering.

2 DESCRIPTION OF CN20 AND ITS ASSOCIATED BRC

CN20 is an irregular infrared dust bubble of about 9 arcmin in size centred at RA 17^{h}44^{m}39^s.2; Dec. −28°02′02″ (J2000) (Churchwell et al. 2007). Fig. 1(left) shows a two-colour composite *Spitzer* image of CN20 (8 μm in cyan and 24 μm in red). The green contours represent the 870-μm emission extracted from the APEX Telescope Large Area Survey of the Galaxy (ATLASGAL; Schuller et al. 2009). The 8 μm emission (GLIMPSE; Benjamin et al. 2003), which traces the photodissociation region (PDR), exhibits an elongated morphology along the RA axis opened towards the western and eastern borders. The 24 μm emission (MIPSGAL; Carey et al. 2009), which might be associated with very small grains, shows a conspicuous nebulosity of about 1 arcmin in size towards the centre of the bubble. This nebulosity shows a semishell-like morphology opening towards the northern border with a point-like source at its centre (clearer in Fig. 2). The 870-μm emission presents a clumpy appearance and shows a clear correlation with the 8-μm emission surrounding the periphery of CN20. In particular, the most striking condensation located towards the southern border of CN20 harbours the ATLASGAL source AGAL000.631+00.604 (Contreras et. al 2013). At 8 μm, the most conspicuous feature is a bright curved filament that encompasses the northern border of the above-mentioned submillimetre source. This correspondence is characteristic of a bright-rim feature.

Fig. 1(right) shows the H_α emission extracted from the SuperCOSMOS H_α Survey (SHS; Hambly et al. 2001) of the H II region G000.640+0.623 (hereafter G0.64) related to CN20. The diffuse emission that arises from the ionized gas fills the interior of the

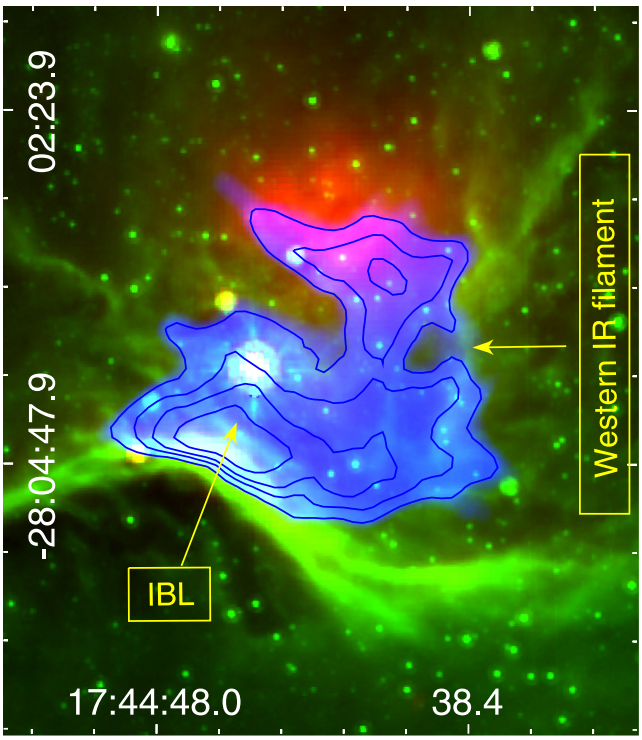

Figure 2. Three-colour composite image of the region of the BRC, with 8 μm in green, 24 μm in red, and the radio continuum emission at 8.9 GHz in blue. Green and red scales go from 60 to 200 MJy sr^{-1} and from 100 to 400 MJy sr^{-1}, respectively. Blue contour levels are at 0.5, 0.7, 0.9 and 1 mJy beam^{-1}.

bubble and is clearly fenced by the emission at 870 μm. This diffuse H II region was first identified by Lockman, Pisano & Howard (1996). These authors found a radio recombination line (RRL) at a radial velocity of about 3.7 ± 0.8 km s^{-1}, which, using a flat rotation model for our Galaxy (with $R = 7.6 \pm 0.3$ kpc and $\theta = 214 \pm 7$ km s^{-1}), corresponds to near and far distances of about 5 and 12 kpc, respectively. The kinematic distance ambiguity can be resolved based on the detection of its associated diffuse optical emission, which makes it unlikely that this H II region is located at the far distance. Thus, in what follows we assume 5 kpc as the distance to CN20.

Fig. 1(left) shows in blue contours the radio continuum emission at 1.4 GHz as extracted from the NRAO VLA Sky Survey (NVSS; Condon et al. 1998). In particular, the contours show the position of the radio source NVSS 17442-280421, which is located in projection onto the illuminated border of AGAL000.631+00.604. It is possible that this emission could arise from the ionized gas typically found at the border of BRCs, but the angular resolution of the NVSS survey prevents a definitive conclusion on this issue.

In this paper, we characterize the uncatalogued BRC located at the southern border of the infrared dust bubble CN20. We also search for evidence of triggered star formation through the RDI mechanism, based on new radio continuum observations at 8.9 GHz carried out with the JVLA and on new molecular line data obtained using the ASTE.

3 OBSERVATIONS AND DATA REDUCTION

3.1 Radio continuum observations

The radio continuum observations towards the BRC were performed in a single field (indicated by the yellow box in Fig. 1(left)) with the JVLA[1] in its DnC configuration, on 2014 September 19 (project ID:14B-069) for a total of 28 min on-source integration time. We used the wideband 8–12 GHz receiver system centred at 9.5 and 10.5 GHz, which consists of 16 spectral windows with a bandwidth of 128 MHz each, spread into 64 channels. The data were processed through the VLA CASA Calibration Pipeline. The source 3C286 was used for primary flux density and bandpass calibration, while phases were calibrated with J1744-3116. We improved the quality of the calibrated data by applying extra flagging before imaging. Visibilities were weighted by applying a robust parameter of 0.5 in MIRIAD, which allowed us to obtain the same sensitivity as with natural weighting but with a better beam shape (Briggs 1995). The image deconvolution was performed with the task CLEAN in MIRIAD. Finally, we reconstructed an image centred at 8.9 GHz with a bandwith of 2 GHz. The resulting synthesized beam has a size of 13 arcsec × 5.3 arcsec, and the rms noise of the final map is about 24 μJy beam^{-1}.

3.2 Molecular observations

The molecular line observation was carried out on 2015 August 28 with the 10 m ASTE (Ezawa et al. 2004). We used the DASH345 GHz band receiver, which is a two-single-band SIS receiver remotely tunable in the LO frequency range of 324–372 GHz. We simultaneously observed a single pointing of ^{13}CO J = 3–2 at 330.588 GHz and of CS J = 7–6 at 342.883 GHz towards RA $17^{h}44^{m}46^{s}.4$; Dec. $-28^{\circ}04'58''$ (J2000). The integration time was 120 s. We used the XF digital spectrometer with the bandwidth and spectral resolution set to 128 MHz and 125 kHz, respectively. The velocity resolution was 0.11 km s^{-1}, and the half-power beamwidth (HPBW) was about 22 arcsec for both observed molecular lines. The system temperature varied from $T_{sys} = 150$ to 300 K. The main beam efficiency was about 0.65. The resulting rms noise of the observations was about 0.06 K for both transitions.

[1] The Very Large Array of the National Radio Astronomy Observatory is a facility of the National Science Foundation operated under cooperative agreement by Associated Universities, Inc.

4 RESULTS AND DISCUSSION

4.1 The radio continuum emission towards the bright-rimmed cloud

Fig. 2 shows a three-colour composite image of the region of the BRC with the 8-μm emission displayed in green, the 24-μm emission in red, and the radio continuum emission at 8.9 GHz in blue. The new higher-sensitivity and higher-angular-resolution radio image shows that the radio emission is characterized by an irregular morphology dominated by a bright arc towards the south. Interestingly, this curved feature perfectly encompasses the outermost layer of the photon-dominated region of the clump detected at 8 μm. The morphological and spatial agreement between the radio and IR features suggests that this radio emission corresponds to the ionized boundary layer (IBL) of the BRC. Fig. 2 also shows that the radio continuum emission also encompasses three infrared structures, namely the above-mentioned BRC towards the south, the bulk of emission at 24 μm to the north, and a filamentary structure seen at 8 μm towards the west.

In order to analyse the nature of the radio emission, we estimate the spectral index between 1.4 and 8.9 GHz using the flux density of 61 mJy tabulated in the NVSS Catalogue at 1.4 GHz, and the estimated value derived from our observations at 8.9 GHz. The radio image at 8.9 GHz was convolved to the lower angular resolution of the NVSS image (∼45 arcsec), and rebinned to the same pixel size. The flux density at 8.9 GHz was estimated as 147 mJy. Thus, a spectral index α of 0.5 ± 0.2 ($S_\nu \sim \nu^\alpha$) was derived, which is consistent with thermal radiation with a relatively high optical depth.

4.1.1 The ionizing star candidates

Fig. 3 shows the H$_\alpha$ emission distribution extracted from the SuperCOSMOS H$_\alpha$ Survey (SHS; Hambly et al. 2001). The blue and green contours represent the radio continuum emission at 8.9 GHz and the 870-μm emission, respectively. Radio continuum and H$_\alpha$ emissions are spatially correlated towards the west, where the 870-μm emission is below 0.02 Jy beam^{-1}. Towards this region, conspicuous bright compact patches in the H$_\alpha$ emission can be seen. It is important to note that clusters of ionizing stars typically have this appearance. Thus, this region would be a good candidate to harbour the ionizing stars responsible for originating the IBL. However, the projected positions of these patches do not seem to generate the morphology of the BRC.

On the other hand, the IBL radio feature is not detected in the H$_\alpha$ emission, probably because of extinction effects originating in the foreground dense clump traced at 870 μm. This might suggest that the ionizing star is illuminating the BRC from behind, along the line of sight.

A search for the ionizing star(s) responsible for the radio continuum emission in the region using the available OB-type stars

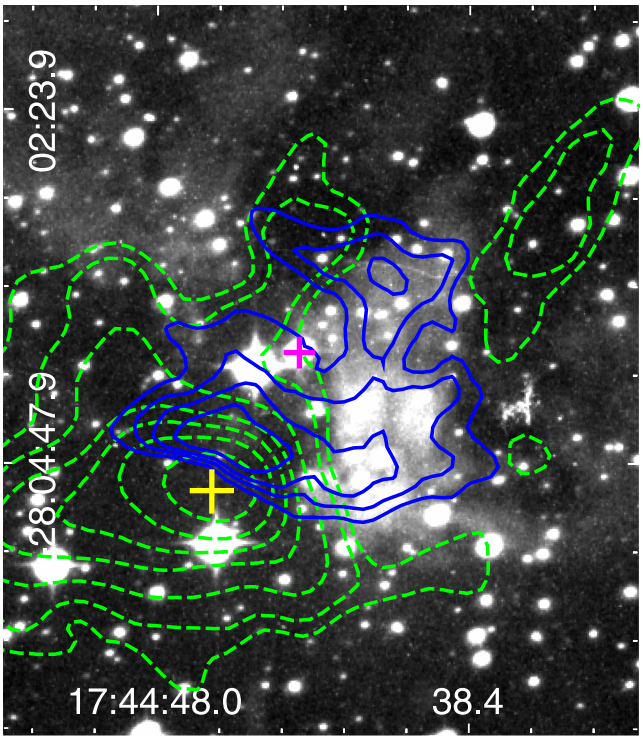

Figure 3. H_α emission distribution extracted from the SuperCOSMOS H_α Survey. The blue and green contours represent the radio continuum emission at 8.9 GHz and the 870-μm emission, respectively. Blue and green contour levels are at 0.5, 0.7, 0.9 and 1 mJy beam^{-1}, and at 0.02, 0.08, 0.15, 0.2, 0.3, 0.4 and 0.6 Jy beam^{-1}, respectively. The magenta cross indicates the position of the ionizing star candidate. The yellow cross represents the pointing of the ASTE observations.

catalogues (e.g. Maiz-Apellaniz et al. 2013, 2004; Reed 2003) was unsuccessful. Therefore, we searched for candidate stars following the *BJHK* colour–colour criterion proposed by Comerón & Pasquali (2012). We considered the near-IR sources of the *JHK* UKIDSS catalogue (Lucas et al. 2008) in an area of 40 arcsec × 40 arcsec centred at RA $17^h44^m43^s$; Dec. $-28°03'53''$ (J2000). We applied a limiting magnitude of $K_S = 11.0$ to the sample in order to reduce the number of early-type stars in the background of the CN20 infrared bubble. This limit corresponds to $M_K = -3.05$ (Martins & Plez 2006) at a distance of 5 kpc, assuming a canonical foreground extinction of $A_V \sim 1$ per kpc. In order to apply the colour–colour criterion we used the UKIDSS sources with associated *B* magnitudes, which were extracted from the NOMAD1 catalogue (Zacharias et al. 2004). The only source in the studied region that fits the selection criteria is NOMAD1 0619-0748987 (magenta cross in Fig. 3). Considering its tabulated $K_S = 10.972$ mag and its associated visual extinction $A_V \sim 7$ (obtained from a $(H - K_S)$ versus $(J - H)$ colour–colour diagram), we derive $M_K = -3.3$, which following the work of Martins & Plez (2006) is in agreement, within errors, with a star of spectral type O9V.

We also independently derived the predicted spectral type of the ionizing star based on the number N_{UV} of UV ionizing photons needed to keep a given amount of gas ionized, which is given by Chaisson (1976) as $N_{UV} = 0.76 \times 10^{47} T_4^{-0.45} \nu_{GHz}^{0.1} S_\nu D_{kpc}^2$, where T_4 is the electron temperature in units of 10^4 K, D_{kpc} is the distance in kpc, ν_{GHz} is the frequency in GHz, and S_ν is the measured total flux density in Jy. Assuming that $T_4 = 1$ and considering the integrated flux density of 147 mJy at 8.9 GHz, we obtain $N_{UV} \sim 3.5 \times 10^{47}$ ph s^{-1}, which is in agreement, within errors, with the tabulated value of $N_{UV} \sim 3.6 \times 10^{47}$ ph s^{-1} for an O9.5V spectral type (Martins & Plez 2006). Given that the two independent estimates of the spectral type of the ionizing star are in agreement, we suggest that NOMAD1 0619-0748987 is a good candidate to be at least one of the ionizing stars in the region. Moreover, the fact that the star is located towards the centre of the radio emission supports this conjecture.

4.2 The bright-rimmed cloud characterization

4.2.1 The ionized boundary layer

Based on the radio continuum emission of the IBL we can estimate the electron density of the layer and the ionizing photon flux impinging upon the illuminated face of the BRC. We estimate for the IBL an integrated flux density at 8.9 GHz of about 45 mJy.

Assuming that all of the ionizing photon flux is absorbed within the IBL, we determined the photon flux, Φ, and the electron density, n_e, using the equations detailed by Lefloch, Lazareff & Castets (1997) and modified by Thompson et al. (2004):

$$\Phi = 1.24 \times 10^{10} S_\nu T_e^{0.35} \nu^{0.1} \theta^{-2} [\mathrm{cm^{-2}\,s^{-1}}] \quad (1)$$

$$n_e = 122.21 \left(\frac{S_\nu T_e^{0.35} \nu^{0.1}}{\eta R \theta^2} \right)^{1/2} [\mathrm{cm^{-3}}], \quad (2)$$

where S_ν is the integrated flux density in mJy, ν is the frequency in GHz, θ is the effective angular diameter over which the flux density is integrated in arcseconds, ηR is the shell thickness in pc, and T_e is the electron temperature in K. Assuming an average electron temperature of about 10^4 K and $\eta = 0.2$ (Bertoldi 1989), and considering an effective θ of about 60 arcsec and a clump radius of $R \sim 44$ arcsec (about 1 pc at a distance of 5 kpc), we derive values for the photon flux and electron density of $\Phi \sim 4.8 \times 10^9$ cm^{-2} s^{-1} and $n_e \sim 176$ cm^{-3}. The main sources of error in the electron density estimate come from the assumption on η and from the uncertainty in the distance. When combined, these give an error of about 50 per cent.

In spite of the large error, the mean electron density value obtained for the IBL is significantly higher than the critical value of $n_e \sim 25$ cm^{-3}, above which an IBL is able to develop around a molecular clump (Lefloch & Lazareff 1994). This reinforces the hypothesis that the clump is being photoionized by a nearby massive star. However, it is not clear to what extent the ionization has influenced the evolution of the cloud, and what role, if any, it played in triggering star formation.

On the other hand, we can also estimate the spectral type for the ionizing star based on the above-derived IBL photon flux by assuming a star located at the position of the source NOMAD1 0619-0748987, which is at a projected distance of about 1 pc from the BRC (see magenta cross in Fig. 3). At this distance, the ionizing photon flux collected by the IBL represents about 12 per cent of that emitted by the star. Thus, we derived a number of UV ionizing photons, N_{UV}, for the exciting star of about 5.1×10^{47} ph s^{-1}, which suggests that the spectral type of the ionizing star would be between a O9V and a O9.5V (Martins & Plez 2006), in good agreement with the results of Section 4.1.1.

4.2.2 Dust properties of the bright-rimmed cloud

The characterization of the neutral material of the BRC allows us to evaluate the influence that the ionization front may have had on the formation of a new generation of stars. *Herschel* observations, with their widespread wavelength coverage, provide a useful tool

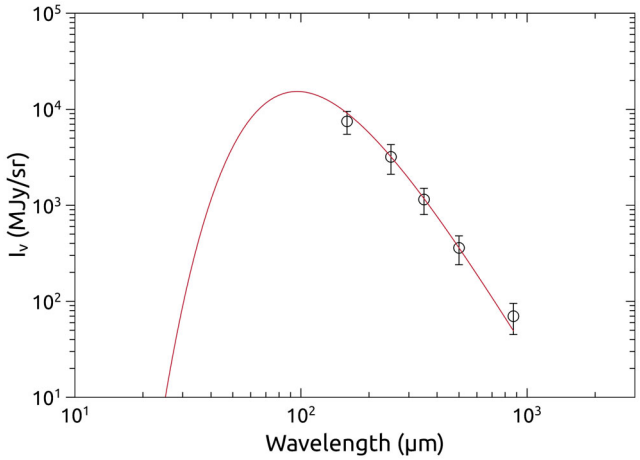

Figure 4. Best-fit to the spectral energy distribution of the bright-rimmed cloud in the submillimetre range using *Herschel* data at 160, 250, 350 and 500 μm and ATLASGAL data at 870 μm.

for studying the dust properties of the interstellar medium (ISM). The spectral energy distribution (SED) fitting at these wavelengths has been widely used to reveal the physical properties of molecular clouds, such as the dust temperature, $T_{\rm dust}$, and the H_2 column density. Assuming dust emission in the optically thin regime, the surface brightness, I_ν, can be expressed as a greybody function for a single temperature:

$$I_\nu = \kappa_{\nu 0}(\nu/\nu_0)^\beta B_\nu(T_{\rm dust})\mu m_{\rm H} N({\rm H_2}), \quad (3)$$

where $B_\nu(T_{\rm dust})$ is the blackbody function for a dust temperature $T_{\rm dust}$, μ is the conversion factor from H_2 to total gas mass, assumed to be 2.8 (e.g. Sadavoy et al. 2013) with a helium abundance of about 25 per cent, $m_{\rm H}$ is the atomic hydrogen mass, and $\kappa_{\nu 0}(\nu/\nu_0)^\beta$ is the dust opacity per unit mass, where $\kappa_{\nu 0}$ is assumed to be 0.1 cm^2 g^{-1} at 1 THz (Beckwith et al. 1990) under a gas-to-dust ratio of 100 and $\beta = 2$ (Anderson et al. 2012).

In order to perform the SED fitting with $T_{\rm dust}$ and $N(H_2)$ as free parameters, we estimated the surface brightness of the clump at five wavelengths, using level 2 (with PASSED status) *Herschel* public data (OBsId 1342204102 and 1342204103) at 160, 250, 350 and 500 μm, and the tabulated flux at 870 μm for the associated ATLASGAL source AGAL000.631+00.604. The *Herschel* data were smoothed to the same angular resolution of 36 arcsec, which is the one corresponding to the 500-μm band. The estimate of the infrared fluxes was carried out in a region the size of the ATLASGAL source ($R_{\rm eff} \sim 44$ arcsec). A background subtraction for each image was carried out using several reference areas away from the bubble.

The free parameters were determined by minimizing the χ^2 between the observed fluxes and those given by equation (3), using the MPFITS package (Markwardt 2009) (see Fig. 4). We derived average values of $T_{\rm dust} = (25 \pm 2)$ K and $N(H_2) = (1.4 \pm 0.3) \times 10^{22}$ cm^{-2}. The mass and the volume density, $n(H_2)$, of the BRC were estimated as $(5.2 \pm 2.1) \times 10^3$ M$_\odot$ and $(3.1 \pm 1.5) \times 10^5$ cm^{-3}.

4.2.3 *The molecular gas towards the bright-rimmed cloud*

Fig. 5 shows the ^{13}CO J = 3–2 (upper panel) and CS J = 7–6 (bottom panel) spectra obtained towards RA 17$^{\rm h}$44$^{\rm m}$46$^{\rm s}$.4; Dec. −28°04′58″ (J2000), in positional coincidence with the emission peak of the ATLASGAL source AGAL000.631+00.604 (see yellow star in Fig. 1-left). The ^{13}CO J = 3–2 exhibits a single component

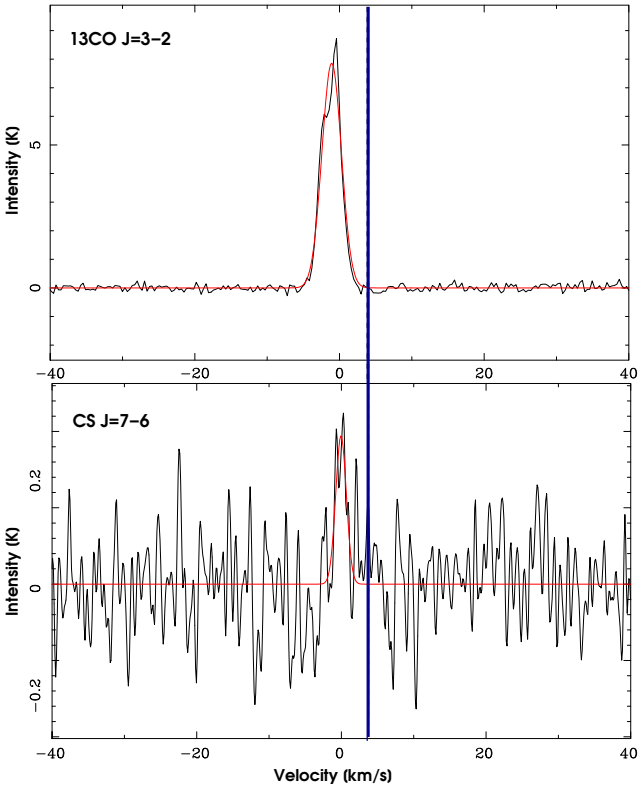

Figure 5. ^{13}CO J = 3–2 (upper panel) and CS J = 7–6 (bottom panel) spectra obtained towards the central position of the ATLASGAL source AGAL000.631+00.604 (see star in Fig. 1-left). The single-component Gaussian fits are shown in red. The vertical line marks the central velocity of the RRL related to G0.64. All velocities are in the local standard of rest.

centred at $V_{\rm LSR} \sim -0.7$ kms^{-1} with an intensity peak of 8.3 K and a line width $\Delta v \sim 3.2$ kms^{-1}. The profile does not show evidence of broadening, which would be expected in a perturbed gas. The central velocity of the component exhibits a shift of about 4 kms^{-1} towards lower velocities with respect to the RRL velocity of G0.64 (Lockman et al. 1996), which suggests that the BRC is located along the line of sight between us and CN20. Thus, the ionizing star would be illuminating the farther border of the clump, which would explain the non-detection of H_α emission related to the IBL.

Assuming local thermodynamic equilibrium (LTE) conditions, it is possible to set $T_{\rm ex} = T_{\rm dust} = 25$ K (see Section 4.2.2) and to derive the ^{13}CO column density from

$$N(^{13}{\rm CO}) = 8.28 \times 10^{13} {\rm e}^{\frac{h\nu}{kT_{\rm ex}}} \frac{T_{\rm ex} + 0.88}{1 - \exp(\frac{-h\nu}{kT_{\rm ex}})} \int \tau_{13} {\rm d}v \quad (4)$$

(e.g. Buckle, Curtis & Roberts 2010), where for the J = 3–2 transition $h\nu/k = 15.87$. Taking into account that the ^{13}CO J = 3−2 spectrum does not show evidence of self-absorption and/or saturation, we can consider this transition to be optically thin, and the following approximation can be used:

$$\int \tau {\rm d}v = \frac{1}{J(T_{\rm ex}) - J(T_{\rm BG})} \int {\rm T_{mb}} {\rm dv}, \quad (5)$$

with

$$J(T) = \frac{h\nu/k}{\exp(\frac{h\nu}{kT}) - 1}, \quad (6)$$

where $T_{\rm BG} = 2.7$ K and $\int {\rm T_{mb}} {\rm dv} \sim 26$ K kms^{-1}.

From the estimated $N(^{13}CO) \sim 1.2 \times 10^{16}$ cm^{-2}, and assuming the $[H_2]/[^{13}CO]$ ratio to be 77×10^4 (Wilson & Rood 1994), we derive an H_2 column density, $N(H_2) \sim 9.2 \times 10^{21}$ cm^{-2}, in agreement with the results of Section 4.2.2.

The CS J = 7–6 spectrum shows a single component centred at about -0.1 kms^{-1}, with an intensity peak of 0.3 K and a $\Delta v \sim 1.5$ kms^{-1}. The detection of CS J = 7–6 suggests the presence of high-density gas in the interior layers of the BRC.

4.3 Triggered star formation within the bright-rimmed cloud?

It is not easy to identify triggered star formation through the RDI mechanism . Triggering is usually inferred by correlating particular stars with some feedback-driven structure. Usually, the spatial distribution of the newly formed stars and eventually some age gradient relative to the ionization front are considered in order to discern whether triggering is plausible. In the case of the RDI mechanism, a useful way to test whether this process is occurring in the interior of a molecular clump is to evaluate the pressure balance between the ionized gas of the IBL and the neutral gas of the illuminated molecular cloud.

4.3.1 Young stellar object population

We identified potential young stellar objects (YSOs) in the region following the colour criterion proposed by Gutermuth et al. (2009) based on *Spitzer* data. Using the *Spitzer* Catalogues, Glimpse II Spring 08 and MIPSGAL at 24 μm, we searched for candidate sources in a box of size ∼ 8 arcmin centred at RA $17^h44^m43^s.3$; Dec. $-28°04'00''.6$ (J2000), discarding sources with 1σ error ≥ 0.2 mag. Following Gutermuth et al. (2009), we excluded sample contaminants such as star-forming galaxies, broad-line active galactic nuclei, unresolved knots of shock emission and resolved polycyclic aromatic hydrocarbon (PAH) emission. The classification scheme proposed by the authors additionally includes three phases, using 2MASS data in order to identify more YSO candidates (YSOc). However, as the infrared bubble CN20 is much farther away than the sources analysed in the study of Gutermuth et al. (2009), 2MASS photometry would be severely affected by foreground interstellar extinction, inducing heavy contamination from the foreground field stars. Thus, we found two Class I and 15 Class II YSOc in the region, which are displayed in Fig. 6. The spatial distribution of Class II YSOc does not show any particular concentration towards the BRC, with only four of them placed in projection onto the molecular condensation. Interestingly, among the two Class I YSOc in the region, one is spatially coincident with the photon-dominated region related to the BRC, which might suggest that a process of triggered star formation is starting in the clump.

In the literature there is some observational evidence (e.g. Ikeda et al. 2008; Chauhan et al. 2009; Smith et al. 2010) that triggered star formation in BRCs should exhibit an age gradient, with the youngest YSOs deeply embedded in the cloud, and the older ones close to the rim of the cloud or distributed inside the expanding H II region. In addition, Sugitani et al. (2000) showed that YSOs formed inside BRCs tend to lie close to the line joining the centre of mass of the cloud to the ionizing star, in agreement with Bisbas et al. (2011), who showed, based on numerical simulations, that star formation in a BRC is concentrated in a dense filament along the axis of symmetry of the cloud, some distance behind the ionization front. In our case, if we consider the three YSOc located in projection near the IBL (assuming that the Class II YSOc are related to the BRC; see Fig. 6), the older ones (Class II) are located closer to the ionizing star than the youngest source (Class I), which would suggest, despite the scarce statistics, an age gradient. However, the spatial distribution of these YSOc does not show any particular concentration onto the axis of symmetry of the cloud. Thus, this BRC does not exhibit clear evidence that the star formation within has been triggered.

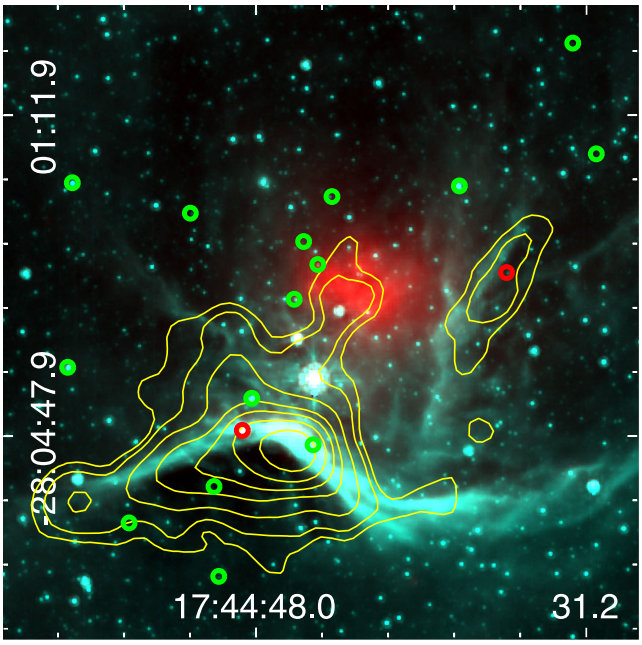

Figure 6. *Spitzer* two-colour image (8 μm in cyan and 24 μm in red) of the bright-rimmed cloud region. Cyan and red scales go from 60 to 200 MJy sr^{-1} and from 100 to 400 MJy sr^{-1}, respectively. The yellow contours represent the ATLASGAL emission at 870 μm. Contour levels are at 0.02, 0.08, 0.15, 0.2, 0.3, 0.4 and 0.6 Jy beam^{-1}. The red and green circles represent the Class I and Class II young stellar objects, respectively.

4.3.2 Testing the radiation-driven implosion mechanism through a pressure-balance analysis

An analysis of the balance between the external and internal pressures, P_{ext} and P_{int} respectively, provides useful information about the influence of the ionization front on the evolution of the BRC. Considering the results of previous sections and following Morgan et al. (2004), the pressures are defined as

$$P_{int} \simeq \sigma^2 \rho_{int}, \quad (7)$$

$$P_{ext} = 2\rho_{ext} c^2, \quad (8)$$

where σ^2 is the square of the velocity dispersion, defined as $\sigma^2 = \Delta v^2/(8 \ln 2)$, with Δv the line width taken from our observations of the ^{13}CO J = 3–2 transition, ρ_{int} is the mass density of the clump, ρ_{ext} is the mass density within the IBL (considering electrons and protons), and $c \sim 11.4$ km s^{-1} is the isothermal sound speed in the ionized interclump gas (e.g. Bertoldi 1989; Urquhart et al. 2006). In order to estimate the ionized gas pressure for the IBL, we considered the electron density calculated in Section 4.2.1 and estimated ρ_{ext}, obtaining $P_{ext}/k_B = (5.4 \pm 2.5) \times 10^6$ cm^{-3} K, which is among the lowest external pressure values derived in similar regions (see e.g. Morgan et al. 2004). In order to estimate the internal pressure of the

condensation, we used the H_2 volume density, $n(H_2)$, calculated in Section 4.2.3, and estimated $\rho_{\rm int}$, yielding $P_{\rm int}/k_{\rm B} = (1.2 \pm 0.5) \times 10^8$ cm^{-3} K.

The comparison of the two pressures reveals that $P_{\rm int} > P_{\rm ext}$ by more than one order of magnitude, which suggests, even considering errors, that the ionization front has stalled at the surface of the clump, probably until the effects of mass evaporation and increasing recombination within the IBL raise the ionized gas pressure to equilibrium with the interior pressure (Lefloch & Lazareff 1994). This result shows that it is unlikely that a shock is propagating farther into the condensation, meaning that the RDI mechanism is not operating in this clump.

We wonder whether triggered star formation could occur in the future in this BRC. Bisbas et al. (2011) give an expression for the critical ionizing photon flux arriving at a BRC, $\phi_{\rm CRIT} \sim 6 \times 10^{13}\,{\rm cm^{-2}\,s^{-1}} \times (M_{\rm CLOUD}/{\rm M_\odot})^{-3}$: above this value the cloud is simply dispersed, without any star formation being triggered. In our case, the estimated ionizing photon flux, $\phi \sim 4.8 \times 10^9\,{\rm cm^{-2}\,s^{-1}}$ (see Section 4.2.1), is several orders of magnitude higher than the critical one, $\phi_{\rm CRIT} \sim 4 \times 10^2\,{\rm cm^{-2}\,s^{-1}}$, which suggests that triggered star formation will not occur in this illuminated clump.

5 SUMMARY

We have presented new radio continuum observations at 8.9 GHz obtained using the Karl Jansky VLA and new molecular observations at the ^{13}CO J = 3–2 and CS J = 7–6 transitions obtained using the ASTE towards an uncatalogued BRC located at the border of the infrared dust bubble CN20. The molecular observations together with *Herschel* data show the presence of a warm and dense illuminated clump. The high angular resolution and sensitivity of the new radio continuum data have revealed an arc-like radio filament in excellent correspondence with the illuminated border of the BRC. We estimated an electron density for this IBL of 176 cm^{-3}, which is several times higher than the critical density above which an IBL can form and be maintained. From a pressure-balance analysis between the IBL and the molecular gas, we suggest that the ionization front has stalled at the surface of the molecular condensation, and therefore that the radiative-driven implosion mechanism will not be operating in this BRC. We have also studied the star formation activity in the region based on colour–colour criterion. The spatial distribution of the YSOc does not show evidence of a triggered origin.

ACKNOWLEDGEMENTS

The ASTE project is led by Nobeyama Radio Observatory (NRO), a branch of the National Astronomical Observatory of Japan (NAOJ), in collaboration with the University of Chile, and Japanese institutes including the University of Tokyo, Nagoya University, Osaka Prefecture University, Ibaraki University, Hokkaido University, and the Joetsu University of Education. MO, EG and SP are members of the Carrera del Investigador Científico of CONICET, Argentina. This work was partially supported by grants awarded by CONICET, ANPCYT and UBA (UBACyT) from Argentina. MR wishes to acknowledge support from FONDECYT (Chile) grant no. 1140839. SP is grateful to Dr T. Okuda for support received during the observations.

REFERENCES

Anderson L. D. et al., 2012, A&A, 542, A10
Beckwith S. V. W., Sargent A. I., Chini R. S., Guesten R., 1990, AJ, 99, 924
Benjamin R. A. et al., 2003, PASP, 115, 953
Bertoldi F., 1989, ApJ, 346, 735
Bisbas T. G., Wünsch R., Whitworth A. P., Hubber D. A., Walch S., 2011, ApJ, 736, 142
Briggs D. S., 1995, BAAS, 27, 112.02
Buckle J. V. et al., 2010, MNRAS, 401, 204
Carey S. J. et al., 2009, PASP, 121, 76
Chaisson E. J., 1976, in Frontiers of Astrophysics, Harvard Univ. Press, Cambridge, MA and London, p. 259
Chauhan N., Pandey A. K., Ogura K., Ojha D. K., Bhatt B. C., Ghosh S. K., Rawat P. S., 2009, MNRAS, 396, 964
Churchwell E. et al., 2006, ApJ, 649, 759
Churchwell E. et al., 2007, ApJ, 670, 428
Comerón F., Pasquali A., 2012, A&A, 543, A101
Condon J. J., Cotton W. D., Greisen E. W., Yin Q. F., Perley R. A., Taylor G. B., Broderick J. J., 1998, AJ, 115, 1693
Contreras Y. et al., 2013, A&A, 549, 45
Dale J. E., Haworth T. J., Bressert E., 2015, MNRAS, 450, 1199
Ezawa H., Kawabe R., Kohno K., Yamamoto S., 2004, Proc. SPIE, 5489, 763
Gritschneder M., Burkert A., Naab T., Walch S., 2010, ApJ, 723, 971
Gutermuth R. A., Megeath S. T., Myers P. C., Allen L. E., Pipher J. L., Fazio G. G., 2009, ApJS, 184, 18
Hambly N. C., Davenhall A. C., Irwin M. J., MacGillivray H. T., 2001, MNRAS, 326, 1279
Haworth T. J., Harries T. J., Acreman D. M., 2012, MNRAS, 426, 203
Haworth T. J., Harries T. J., Acreman D. M., Rundle D. A., 2013, MNRAS, 431, 3470
Ikeda H. et al., 2008, AJ, 135, 2323
Kinnear T. M., Miao J., White G. J., Goodwin S., 2014, MNRAS, 444, 1221
Lefloch B., Lazareff B., 1994, A&A, 289, 559
Lefloch B., Lazareff B., Castets A., 1997, A&A, 324, 249
Lockman F. J., Pisano D. J., Howard G. J., 1996, ApJ, 472, 173
Lucas P. W. et al., 2008, MNRAS, 391, 136
Maíz-Apellániz J., Walborn N. R., Galué H. Á., Wei L. H., 2004, ApJS, 151, 103
Maíz-Apellániz J. et al., 2013, Massive Stars: From Alpha to Omega, 198
Markwardt C. B., 2009, in Bohlender D. A., Durand D., Dowler P., eds, ASP Conf. Ser. Vol. 411, Astronomical Data Analysis Software and Systems XVIII. Astron. Soc. Pac., San Francisco, p. 251
Martins F., Plez B., 2006, A&A, 457, 637
Morgan L. K., Thompson M. A., Urquhart J. S., White G. J., Miao J., 2004, A&A, 426, 535
Morgan L. K., Urquhart J. S., Thompson M. A., 2009, MNRAS, 400, 1726
Reed B. C., 2003, AJ, 125, 2531
Reipurth B., 1983, A&A, 117, 183
Sadavoy S. I. et al., 2013, ApJ, 767, 126
Sandford M. T., II, Whitaker R. W., Klein R. I., 1982, ApJ, 260, 183
Schuller F. et al., 2009, A&A, 504, 415
Smith N. et al., 2010, MNRAS, 406, 952
Sugitani K., Ogura K., 1994, ApJS, 92, 163
Sugitani K., Fukui Y., Ogura K., 1991, ApJS, 77, 59
Sugitani K., Tamura M., Ogura K., 1995, ApJ, 455, L39
Sugitani K., Matsuo H., Nakano M., Tamura M., Ogura K., 2000, AJ, 119, 323
Thompson M. A., Urquhart J. S., White G. J., 2004, A&A, 415, 627
Thompson M. A., Urquhart J. S., Moore T. J. T., Morgan L. K., 2012, MNRAS, 421, 408
Urquhart J. S., Thompson M. A., Morgan L. K., White G. J., 2006, A&A, 450, 625
Urquhart J. S., Hoare M. G., Lumsden S. L., Oudmaijer R. D., Moore T. J. T., 2008, in Beuther H., Linz H., Henning T., eds, ASP Conf. Ser. Vol. 387, Astronomical Data Analysis Software and Systems XVIII. Astron. Soc. Pac., San Francisco, p. 381
Urquhart J. S., Morgan L. K., Thompson M. A., 2009, A&A, 497, 789
Wilson T. L., Rood R., 1994, ARA&A, 32, 191
Zacharias N., Monet D. G., Levine S. E., Urban S. E., Gaume R., Wycoff G. L., 2004, BAAS, 36, 1418

This paper has been typeset from a TEX/LATEX file prepared by the author.